Co-pyrolysis of chicken feathers and macadamia 1 nut shells, a promising strategy to create 2 nitrogen-enriched electrode materials for 3 supercapacitor applications 4 5

Peer-reviewed author version

VERCRUYSSE, Willem; Muniz, R.R.; JOOS, Bjorn; HARDY, An; HAMED, Hamid; DESTA, Derese; BOYEN, Hans-Gerd; SAFARI, Momo; MARCHAL, Wouter; VANDAMME, Dries & Schreurs, S (2024) Co-pyrolysis of chicken feathers and macadamia 1 nut shells, a promising strategy to create 2 nitrogen-enriched electrode materials for 3 supercapacitor applications 4 5. In: Bioresource technology, 396 , p. 130417 (Art N° 130417).

DOI: 10.1016/j.biortech.2024.130417
Handle: http://hdl.handle.net/1942/45864

Co-pyrolysis of chicken feathers and macadamia nut shells, a promising strategy to create nitrogen-enriched electrode materials for supercapacitor applications

W. Vercruysse[a], Roman-Muniz R.[a], B. Joos[b], A. Hardy[b], H. Hamed[c], D. Desta[d], H.-G. Boyen[d], Schreurs S.[e], Safari M.[c], Marchal W.[a], Vandamme D.[a]*

[a] UHasselt - Hasselt University, Analytical and Circular Chemistry, Centre for Environmental Sciences (CMK), Institute for Materials Research (imo-imomec), Agoralaan, 3590, Diepenbeek, Belgium

[b] UHasselt - Hasselt University, Design and Synthesis of Inorganic Nanomaterials, Institute for Materials Research (imo-imomec) and Energyville, Agoralaan, 3590, Diepenbeek, Belgium

[c] UHasselt - Hasselt University, Electrochemical Engineering, Institute for Materials Research (imo-imomec) and Energyville, Agoralaan, 3590, Diepenbeek, Belgium

[d] UHasselt - Hasselt University, Nano Structure Physics, Materials physics, Institute for Materials Research (imo-imomec), Agoralaan, 3590, Diepenbeek, Belgium

[e] UHasselt - Hasselt University, Nuclear Technology Centre (NuTeC), Centre for Environmental Sciences (CMK), Agoralaan, 3590, Diepenbeek, Belgium

*Corresponding Author: dries.vandamme@uhasselt.be

To be submitted to:

ACS Sustainable Chemistry & Engineering (2023) (IF 9.2)

Abstract

Global food waste emits large quantities of nitrogen (6.3 Mtons annually) into our environment, acidifying surface waters and reducing the air quality. Among the nitrogen-rich waste streams, waste chicken feathers (CF) stand out with an annual production of 7-10 Mtons. Instead of incinerating or landfilling CF an alternative approach involves pyrolysis converting it into biochar, hereby incorporating nitrogen in a carbon structure and reducing nitrogen emissions. As such, this biochar can serve as a valuable building block for the production of high-quality nitrogen-enriched activated carbons, which find applications as electrode materials in supercapacitors. One strategy to improve the extent of nitrogen incorporation during thermochemical conversion is through co-pyrolysis of nitrogen-rich and lignocellulosic waste streams. As such, this study will investigate the co-pyrolysis of CF with macadamia nut shells (MNS) to create highly porous and nitrogen-rich activated carbons. Additionally, demineralization of the resulting activated carbon will be assessed as a means to improve its electrochemical performance. Co-pyrolysis increased the nitrogen retention during the pyrolysis from 9% to 18% compared to CF pyrolysis. Moreover, the porous characteristics of the blended activated carbons were comparable to pure MNS activated carbon. Demineralization increased both meso-and microporosity of the co-pyrolyzed activated carbon, leading to a specific capacitance of 66 F/g at 1 mV/s in a symmetric supercapacitor. Additionally, this activated carbon outperformed a commercial benchmark when using higher scan rates (20 mV/s) delivering 43 F/g compared to 30 F/g. This superior performance was attributed to the abundance of mesopores in the co-pyrolysis activated carbon, facilitating rapid charge transport. Finally, cycling stability tests demonstrated good stability with 73% of capacitance retention after 10 000 cycles.

1 Introduction

Global food waste emits 6.3 Mtons of nitrogen on an annual basis [1], leading to eutrophication, acidification of surface waters and reductions in air quality that negatively impact our human health [2]. Around 30% of the globally produced food waste originates from meat production [3], poultry production in particular is the source of a large fraction of nitrogen-rich side streams, a substantial fraction of which are chicken feathers (7-10 Mtons annual production [4]). Recently, the scientific community proposed thermochemical conversion (pyrolysis) as a feasible strategy to reduce the nitrogen emission of food waste [3] as an alternative to incineration or landfilling, by incorporating nitrogen into a solid residue, biochar. As such, a valuable product would be created which could be used as a building block for high-value nitrogen enriched activated carbons [5].

Previous research has shown that chicken feathers (CF) can be used as a feedstock for nitrogen-rich activated carbon production. Moreover, it was found that these could be effectively used as adsorbents [6], as anode material in Li-ion batteries [7] or as active material in supercapacitors [6]. However, the direct thermochemical conversion of CF (or other nitrogen-rich biomass streams [8]) is always correlated with a high release of nitrogen (>90%). Therefore, thermochemical conversion strategies which mitigate the emission of nitrogen during the thermochemical conversion of nitrogen-rich biomass feedstocks need to be further investigated.

Co-pyrolysis of nitrogen-rich feedstocks with lignocellulosic biomass is a promising strategy to increase biochar yields [9] and nitrogen retention [10], [11] during pyrolysis. Therefore, co-pyrolyzing CF with a lignocellulosic biomass stream would be a promising strategy to create nitrogen-rich activated carbons, with the intent of applying them for electrochemical energy storage.

Another limitation of biomass-derived activated carbons is the presence of inherent biomass minerals in the activated carbons [12]. Their presence would block pores, which results in decreased adsorption capacities [13], limiting their applicability in supercapacitive devices where large electrolyte sorption capacities are required. Nevertheless, the role of biomass inherent minerals on the capacitive performance is often overlooked in current scientific literature [14] and requires further in-depth study.

The lignocellulosic biomass of choice for co-pyrolysis would be macadamia nut shells (MNS), another type of food waste, as these have proven to be perfectly suitable for the production of highly porous activated carbons which can be applied in high power density supercapacitors [15], [16], [17]. However, conventional MNS-based activated carbons entirely rely on electrochemical-double layer capacitance (EDLC) as charge storage mechanisms their total energy density is therefore limited [18]. As such, nitrogen-rich activated carbons are under investigation, as the presence of the heteroatom (nitrogen) in the carbon framework has positive effects on the material’s pseudocapacitance [19] and electrical conductivity [20]), which results in an increased energy density [21]. Moreover, creating nitrogen-rich activated carbon from nitrogen-rich biomass sources has the additional advantage that a chemical nitrogen doping step can be omitted [22], which improves the inherent sustainable nature of the activated carbon production process [23].

Building on the knowledge obtained in a previous study (ref myself when published), where a highly porous activated carbon was produced from MNS and a highly nitrogenous activated carbon was derived from CF, the symbiosis between both processes and materials is targeted in this follow-up study. Hence, the co-pyrolysis of CF and MNS and activation followed by demineralization to create highly functional activated carbons is explored, followed by a thorough electrochemical evaluation of the created activated carbons.

2 Materials & Methods

2.1 Biomass streams

The biomass streams investigated in this study were CF and MNS. MNS were obtained from Act&Sorb BV (Genk, Belgium). CF were collected from chicken slaughterhouse Schildermans – Pludis NV (Bree, Belgium). Whereupon they were dried to contstant weight at 105 °C. After drying, the biomasses were shredded to 2x2mm using a Retsch SM100 shredder (Retsch, Haan, Germany).

A reference activated carbon commonly applied in supercapacitor electrodes was used in this investigation for comparison (SuperCarb EL-103, Jacobi Carbons AB). Its key properties are described in the table below, Table 1.

Table 1: Reference activated carbon properties of commercial reference material (O calculated by difference, dry basis, $\bar{x} \pm s/\sqrt{n}$, n ≥ 3)

Property	Commercial activated carbon
N (wt%)	0.54 ± 0.09
C (wt%)	99.4 ± 0.4
H (wt%)	0.7 ± 0.1
O (wt%)	< 0.5
Ash (wt%)	0.1 ± 0.1
S_{BET} (m^2/g)	1285
V_{micro} (cm^3/g)	0.61
V_{meso} (cm^3/g)	0.05

2.2 Thermochemical conversion

The pyrolysis and activation experiments were done in an identical set-up as used in previous studies [24,25]. The utilized carbonization and activation parameters are explained in detail in a previous study [26]. In short, the pyrolysis temperature was 700 °C. Physical activation was done using steam at 800 °C, with a steam:biomass ratio of 1:1. All pyrolysis experiments were carried out at least in triplicate using biomass loadings of 40 g (MNS and M50-C50) or 30 g (CF), activations were done in duplicate, using a biochar input of 10 g. After thermochemical conversion, the activated carbons were demineralized using (10% HCl) using an identical methodology as described in a previous study [26]. Activated carbon:solvent mixing ratios were 1:20 (mass activated carbon: vol. solvent) and stirred for 60 min at 80 °C. Next, samples were filtered and washed with hot water until neutral pH to remove residual solvent. Hereafter, the washed activated carbons were dried at 105 °C.

2.3 Sample characterization

Ultimate analysis of the biomass, biochars and activated carbons was performed using a Thermo Electron Flash EA1112 elemental analyzer (ThermoFisher Scientific, Waltham, USA). Calibration was carried out using BBOT ((2,5-bis (5-tert-butyl-benzoxazol-2-yl) thiophene) (pure, ThermoScientific). Ash contents of all samples were determined following ASTM D2866 - 94 [27]. Finally, oxygen content was calculated by difference: O (wt%) = 100 % – C (wt%) – N (wt%) – H (wt%) – S (wt%) – Ash (wt%). Samples were measured at least in triplicate.

Activated carbon's porosity and surface area was determined via N_2 adsorption and desorption experiments physisorption (N_2-isotherms in supplementary information, Figure S1) . The measurements were performed at 77 K using a Tristar II 3020 surface area analyzer (Micromeritics, Norcross, USA). The sample was degassed under nitrogen flow at 150 °C for 16 h prior to measurement to remove any residual moisture and residual volatiles. The specific surface area, micropore volume and meso/macro pore volume were correspondingly estimated via the Brunauer-Emmett-Teller (BET), t-plot method (Carbon Black STSA thickness curve) and Barrett-Joyner-Halenda (BJH) methods.

XPS measurements were performed on powdered activated carbon samples (secured onto a clean aluminum foil) using a commercial electron spectrometer (Physical Electronics, PHI-5600LS, USA). Core-level XPS spectra were obtained using Al-k_a photons (1486.6 eV) provided by a small-spot monochromator system (1 mm spot-size). High-resolution spectra were acquired using a total energy resolution of the spectrometer (photons and electrons) of 0.36 eV full- width at half maximum (FWHM). The spectrometer's binding energy scale was calibrated utilizing an independent Au bulk reference sample ($Au4f_{7/2}$: 84.0 eV). The high-resolution spectra were analyzed using CasaXPS software package accounting for a Shirley-type of background. A numerical least-squares fitting procedure [28] was used for peak fitting. Peak annotation was done following earlier published literature [29].

X-ray fluorescence (XRF) analysis of the activated carbon was done using an S4 Explorer wavelength-dispersive XRF spectrometer (Bruker, Billerica, USA). Powdered samples were measured under He-atmosphere. The observed intensities of the analyzed minerals were compared to a set of universal calibration standards. Elemental concentrations were calculated by applying a correction to the sample matrix (for carbon, based on the CHNS-analysis) and using the EVAL-software (standard less calibration). The reported elements include Al, Ca, Fe, K, Mg, Na, P and S, as these would have the highest impact on the electrochemical performance of the activated carbons due to their relative abundance in the investigated biomass streams.

2.4 Electrochemical evaluation

The activated carbons were tested as electrode materials in symmetrical coin cells using a two-electrode set-up. The slurry composition in this study was 85% activated carbon, 5% carbon black (C-NERGY^{TM} SUPER C45 carbon black, Imerys), and 10% PVDF (Polyvinylidene fluoride powder, Alfa Aesar). After weighing, the electrode components were homogenized by ball milling (Emax ball mill, Retsch GmbH, Haan, Germany) using the following milling protocol: 15 min at 300 RPM, followed by 5 min at 500 RPM. Subsequently, the coatings were blade coated (MSK-AFA-II-220, MTI, Richmond, USA) onto Al-foil using 200 µm wet thickness. Hereafter, coatings were dried (Heratherm AP GH60, Thermo Fisher, Waltham, USA) at 110 °C overnight. All electrode porosities were similar (65-70%) after drying. Coin cells were assembled symmetrically using punches (MSK T-06, MTI, Richmond, USA) with a diameter of 1.5 cm. The used electrolyte was 1 M $LiPF_6$ in EC/DEC. A commercial supercapacitor separator (Dreamweaver Titanium GT 0.45/40) was utilized in the two-electrode coin cells. A reference coconut-shell based commercial activated carbon (SuperCarb EL-103, Jacobi Carbons AB) was incorporated in a reference coin cell as a benchmark.

The coin cells were tested using a biologic battery tester module. Cyclic voltammetry (CV) was done using scan rates of 1, 5, 10, 20, 30, 40, 50, 75 and 100 mV/s from 0 to 2.5 V for 10 cycles. The tenth cycle was used to assess the specific capacitance of the coin cells as in this case a steady-state was assumed. Galvanostatic charge discharge experiments were done in the same voltage window (0-2.5V) and using currents 0.1, 0.2, 0.5, 1, 2 and 5 mA. From these measurements, an alternative value for the specific capacitance of the different coin cells was calculated. Electrochemical impedance spectroscopy (EIS) was recorded over the frequency range of 0.01 to 10 kHz with a voltage amplitude of 5 mV. The cycling stability of the most promising activated carbons was tested for 10 000 cycles at a current density of 1 A/g.

3 Results & Discussion

The pyrolysis experiments showed that the biochar yield of CF was lower (13%) than for MNS (27.5%) and M50-C50 (25.9%), Figure 1. This indicates that the co-pyrolysis of CF and MNS has a positive impact on the retention of solid matter, as the theoretical interpolated retention would have been 20.3% if both biomass streams were pyrolyzed without any interaction. These increased yields are in line with other studies for the co-pyrolysis of nitrogen-rich (microalgae) and lignocellulosic biomass (bamboo) [11]. After pyrolysis, the chars were activated using steam. M50-C50 seemed to have the lowest AC-yields (52% compared to 55% for MNS and 58% for CF). The total process yields ranged therefore from 7.6 for CF to 13.4 for M50-C50 and 15.2% for MNS.

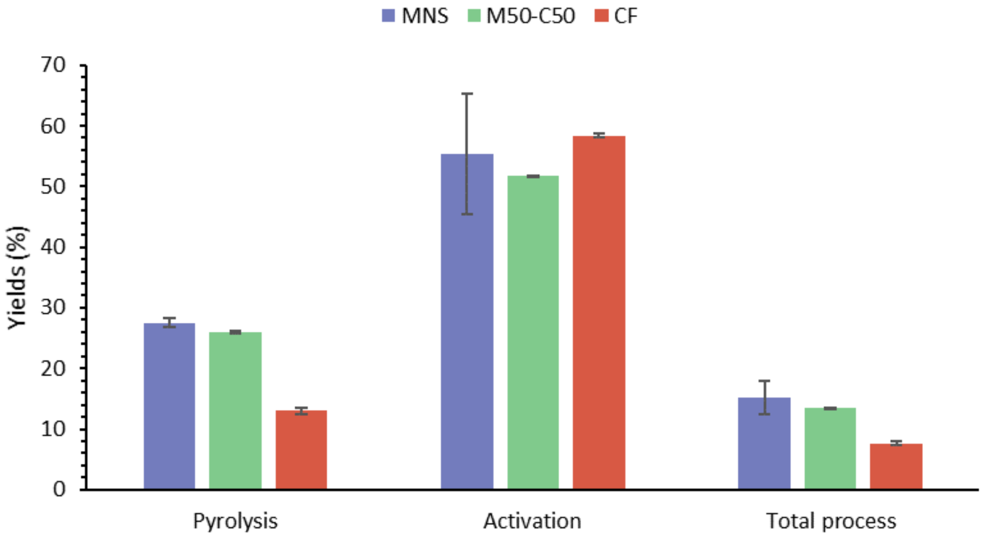

Figure 1: Biochar yields of MNS, M50-C50 and CF

All biomass, biochars and activated carbons were analyzed for their respective elemental composition and ash-contents, Table 2. This was done to assess the effect of co-pyrolysis and activation on the nitrogen-content of the resulting biochar and activated carbons.

Table 2: Ultimate analysis of biomass, biochar and activated carbon (O calculated by difference, dry basis, $\bar{x} \pm s/\sqrt{n}$, $n \geq 3$)

Biomass	**N (wt%)**	**C (wt%)**	**H (wt%)**	**S (wt%)**	**O (wt%)**	**Ash (wt%)**
MNS	0.76 ± 0.04	52.8 ± 0.7	6.1 ± 0.1	n.d.	39.0 ± 0.8	1.3 ± 0.1
M50-C50	7.5 ± 0.3	53.5 ± 0.2	6.92 ± 0.01	1.48 ± 0.06	29.1 ± 0.4	1.51 ± 0.06
CF	14.6 ± 0.1	51.4 ± 0.4	7.53 ± 0.05	2.20 ± 0.05	23.3 ± 0.4	1.02 ± 0.02
Biochar	**N (wt%)**	**C (wt%)**	**H (wt%)**	**S (wt%)**	**O (wt%)**	**Ash (wt%)**
MNS	0.87 ± 0.04	90.56 ± 0.02	1.34 ± 0.3	n.d.	1.4 ± 0.4	5.8 ± 0.1
M50-C50	5.4 ± 0.1	82.53 ± 0.06	1.04 ± 0.8	n.d.	5 ± 1	6.0 ± 0.1
CF	10.80 ± 0.06	79.05 ± 0.03	1.33 ± 0.2	n.d.	1.5 ± 0.2	7.34 ± 0.01
AC	**N (wt%)**	**C (wt%)**	**H (wt%)**	**S (wt%)**	**O (wt%)**	**Ash (wt%)**
MNS	0.22 ± 0.01	88.7 ± 0.9	1.33 ± 0.1	n.d.	0.3 ± 1	9.4 ± 0.2
M50-C50	2.61 ± 0.03	83.3 ± 0.7	1.43 ± 0.5	n.d.	2.2 ± 0.9	10.47 ± 0.08
CF	5.19 ± 0.09	81 ± 1	1.27 ± 0.04	n.d.	0.1 ± 1	12.82 ± 0.04
AC-W	**N (wt%)**	**C (wt%)**	**H (wt%)**	**S (wt%)**	**O (wt%)**	**Ash (wt%)**
MNS-W	0.61 ± 0.03	85.9 ± 0.5	1.34 ± 0.04	n.d.	8.0 ± 0.5	4.1 ± 0.2
M50-C50-W	2.76 ± 0.04	79.9 ± 0.8	2.02 ± 0.06	n.d.	11.6 ± 0.8	3.7 ± 0.1
CF-W	4.48 ± 0.02	73.7 ± 0.2	1.25 ± 0.03	n.d.	18.2 ± 0.2	2.40 ± 0.08

The nitrogen retention for M50-C50 during the pyrolysis process doubled compared to the CF pyrolysis, from 9.6 to 18.6% (calculated based on biochar yields and nitrogen contents, data displayed in supplementary material, Figure S2). This could have been caused by Maillard reactions [30] between lignocellulose fragmentation products (e.g., glucose) and protein nitrogen functionalities. The nitrogen retention for the co-pyrolysis was significantly lower than the retention in MNS (31.5%) however, in this case, nitrogen was only present in small quantities which would increase the chances of the occurrence of nitrogen recombination reactions during the pyrolysis of MNS [8]. Ultimately the pyrolysis experiments yielded nitrogen-rich biochar in M50-C50 (5.4% N) and CF (10.8% N). The carbon contents of all biochar increased after pyrolysis, the highest biochar carbon contents were found in MNS (90.6%), followed by M50-C50 (82.5%) and CF (79.1%). These high carbon contents came with low hydrogen contents (<1.5%), indicating that all carbonization and aromatization processes were complete [31]. Moreover, the ash contents of the biochars (5.8 - 7.4

wt%) increased after pyrolysis compared to biomass (1.3 - 1.02 wt%), as ash is not volatized during the pyrolysis process [32].

During the physical activation a large fraction of the nitrogen present in the activated carbons was removed (for CF this was 72%, while for M50-C50 the nitrogen removal increased to 75%). For MNS, only 14% of the biochar N was retained, resulting in a relatively nitrogen-poor activated carbon. Nevertheless, the activated carbons produced from CF and M50-C50 had a higher quantity of nitrogen (4.5 and 2.8% N) compared to the commercial reference (0.5%; Table 1). To discover the speciation of the remaining N-species XPS analyses on the activated carbons were performed, Figure 2.

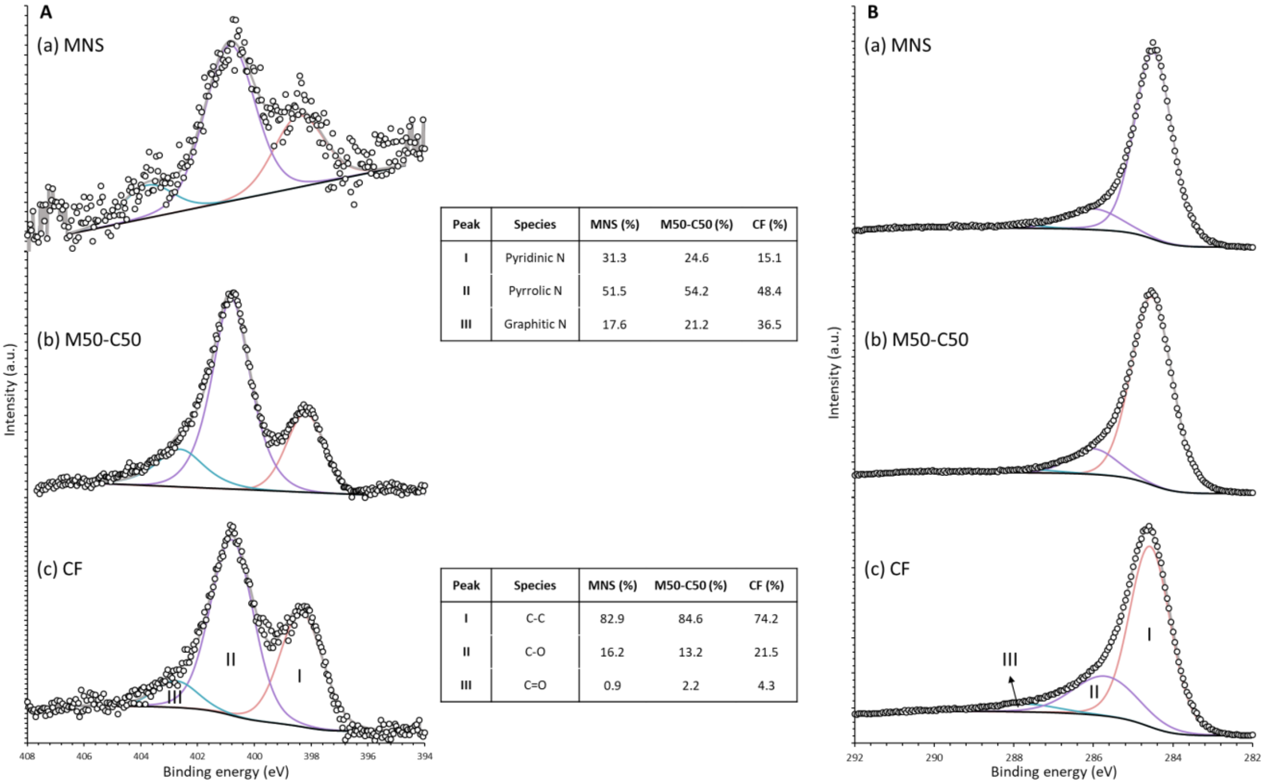

Peak	Species	MNS (%)	M50-C50 (%)	CF (%)
I	Pyridinic N	31.3	24.6	15.1
II	Pyrrolic N	51.5	54.2	48.4
III	Graphitic N	17.6	21.2	36.5

Peak	Species	MNS (%)	M50-C50 (%)	CF (%)
I	C-C	82.9	84.6	74.2
II	C-O	16.2	13.2	21.5
III	C=O	0.9	2.2	4.3

Figure 2: A) N 1s and B) C 1s XPS spectra of activated carbons, the speciation is reported relative to the total measured nitrogen and carbon in de biochar surface

Only heterocyclic nitrogen species were detected in the activated carbons, the other more thermolabile nitrogen-species would be removed during the high-temperature pyrolytic conversion [33] or after physical activation with steam [34]. With increasing quantities of CF in the feedstock the relative amount of graphitic nitrogen in the activated carbons increased, Figure 2A. The largest peak in the N 1s spectrum was attributed to pyrrolic nitrogen for all three activated carbons. Lastly, the content of pyridinic nitrogen was the inverse of graphitic nitrogen, it increased when more lignocellulosic biomass was present in the biomass feedstock. The fixation of nitrogen during thermochemical conversion of lignocellulosic biomass and nitrogen-rich biomass would yield a respectively larger quantity of pyridinic nitrogen and less graphitic nitrogen [30]. It can be concluded that combining MNS and CF leads to an increased nitrogen retention and a relative lower quantity of graphitic N.

The carbon content of the activated carbons, Table 2, was similar compared to their corresponding biochars. Hence, it is assumed that all activated carbons are completely aromatic at this stage of the thermochemical conversion. The speciation of the carbon functionalities was also investigated with XPS, Figure 2B. The largest fraction of carbon (>74% for all of the activated carbons) was of the C-C variety. Next to this, contributions of C-O and C=O species were found for CF, MNS and M50-C50. These could have originated from the activation process which introduces oxygen species on the activated carbon’s surface [35]. This heightened degree of oxygen functionality could have either positive (improved pseudocapacitance [36]) and negative effects (decreased conductivity and occurrence of side-reactions [37]) on the performance of the activated carbon in electrode materials.

Another important activated carbon property is the ash content, i.e., the presence of inorganic compounds. In general, for electrochemical applications very pure (low ash-content) activated carbons are desired, as the present biomass ash could block activated carbon’s pores, which would lead to a lower specific capacitance [13]. Moreover, the presence of inorganic ash can have several negative consequences in activated carbon electrodes, e.g., increased self-discharge, decreased overall gravimetric capacitance or undesired additional charge shuttling effects [14]. CF activated carbon has the highest ash-content, 12.8%, of the three biomass streams, followed by M50-C50 (10.5%) and MNS (9.4%). Therefore, it would be a promising strategy to improve the activated carbon’s future applicability to demineralize the CF-MNS activated carbons using dilute HCl, as this proved to have the highest demineralization efficiency.

After washing of the activated carbons, the activated carbon ash content decreased (>60% removal) significantly. The largest effects were observed for CF where an ash content of 2.4% was achieved after washing, yet the demineralization treatment has also a strong beneficial influence on the M50-C50 and MNS ash contents after washing, respectively 3.7 and 4.1. However, treating the activated carbons with dilute HCl introduced also a large quantity of oxygen functionalities on the carbon surface [38] as a side effect (O contents of respectively 8.0, 11.6 and 18.2% for MNS, M50-C50 and CF). Only small relative decreases in N-content occurred, most likely due to the relative increase in oxygen functionalities rather than extensive removal of nitrogen species in the activated carbons as treatment of activated carbons with HCl, does not affect the organic N-species to a large extent [39].

The ultimate purpose of the physical activation was to create porosity by removing carbon species from the biochar carbon framework. To assess this a nitrogen physisorption experiment of the activated carbons was carried out, Figure 3.

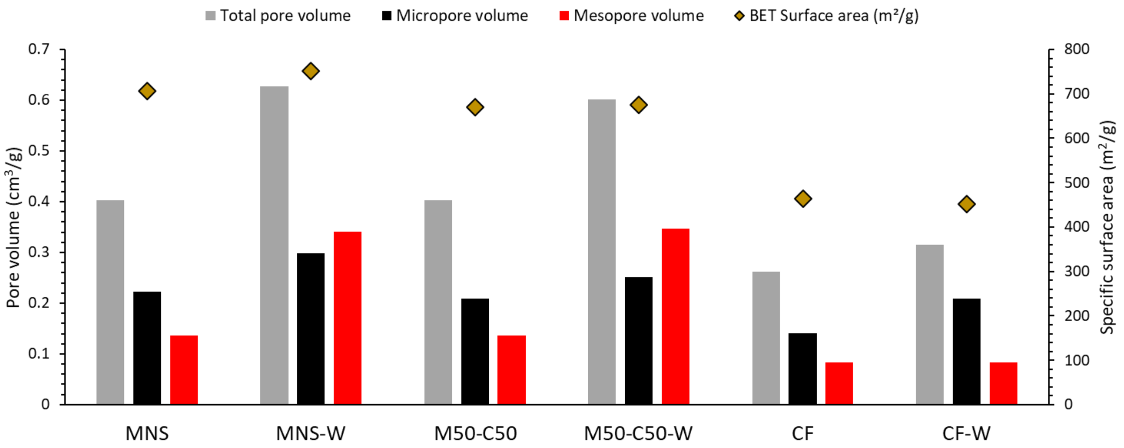

Figure 3: Porous characteristics of the activated carbons as determined by N_2-physisorption experiments

The specific surface area of MNS was highest of the three tested activated carbons with 707 m^2/g, however M50-C50 showed a marginally lower BET surface area of 670 m^2/g. CF had a lower specific surface area of 463 m^2/g. Hence, co-pyrolyzing CF and MNS did not significantly decrease the specific surface area of the activated carbons. The activated carbons were mostly microporous (around 60% of the total pore volume), but also a significant fraction of mesoporosity was present (40%). This distribution could be beneficial for capacitive applications as both pore sizes play a distinctive role in charge-storage processes [40].

After washing the porosity of all activated carbons increased, as observed from the nitrogen physisorption isotherms (Figure S1), the greatest improvements were observed for MNS and M50-C50, for CF the increases were less pronounced. In terms of specific surface area only minor changes were observed after washing, for MNS it increased from 707 to 752 m^2/g, for M50-C50 from 670 to 676 m^2/g and decreased for CF from 463 to 452 m^2/g. However, investigating the total pore volumes of the activated carbons shows a different phenomenon, these were all increased after washing. From respectively 0.402, 0.403 and 0.262 cm^3/g for MNS, M50-C50 and CF to 0.628, 0.602 and 0.316 cm^3/g after washing. For MNS and M50-C50 this was mostly driven by an increase in mesoporosity, while for CF microporosity increased after washing. Compared with the commercial benchmark (Table 1) the specific surface area and microporosity of all the washed and unwashed activated carbons was significantly lower. However, their mesoporosity, especially in the case of MNS-W and M50-C50-W, was increased.

To elucidate the different types of porosity development after washing, XRF analysis was done to determine which metal species were removed from the activated carbons.

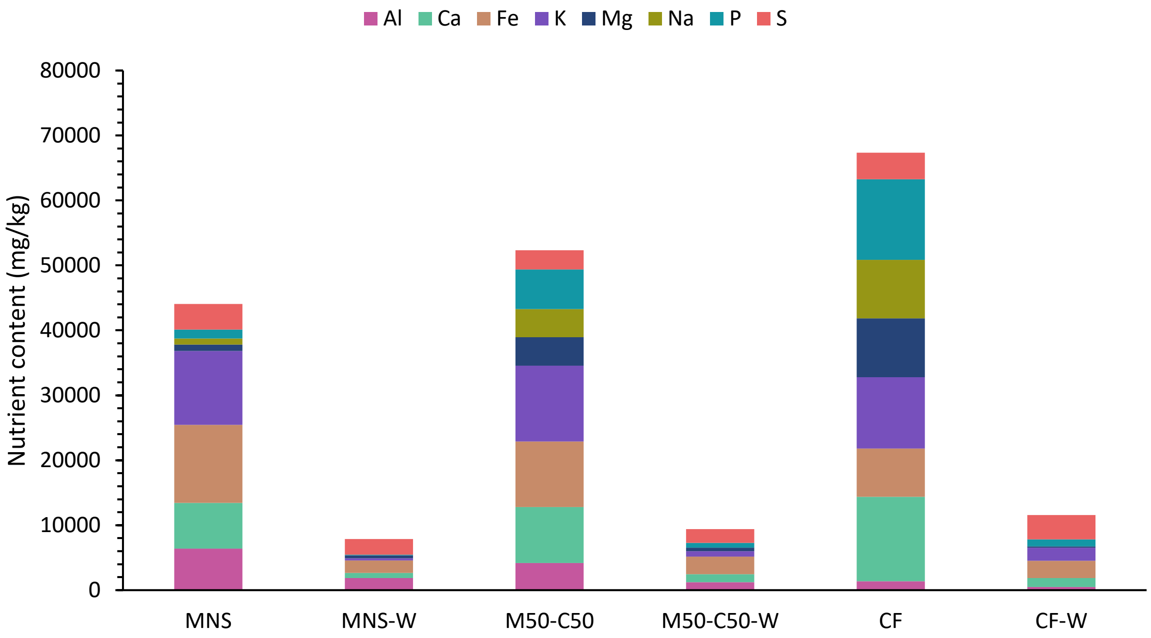

Figure 4: Composition of the ash fraction of pristine and demineralized activated carbons

In terms of mineral composition, the most abundant inorganic compounds in the activated carbons are displayed in Figure 4. For MNS, these were in decreasing order of abundance Fe, K, Al, Ca, S, P, Mg and Na. For CF, the composition was slightly different, with Ca, P, K, Na, Mg, Fe, S and Al. M50-C50 showed a combination of both CF and MNS, which was expected as most minerals do not volatize during the thermochemical conversion processes [32]. For all activated carbons the removal of the different fractions of ash are high (>60% removal of total ash), which explains the heightened porosity for all three activated carbons. The demineralization of MNS and M50-C50 increased their mesoporosity significantly, as this could be due to the opening of blocked pores which were previously not accessible [41]. The large removal of the mineral cations for MNS (Al 71%, Ca 89%, Fe 84%, K 97% and Na 100%) indicated that blocked pores are opened by the removal of the inorganic salts. Similar removals were observed for M50-C50 although the retention was slightly higher for Ca (85% removal), Fe (73% removal) and K (93% removal). For CF, the retentions are slightly higher compared to MNS and M50-C50 for some minerals (Al, Fe and K) or similar for others (Ca, P). Moreover, for Mg the retention decreases significantly with increasing contents of CF in the activated carbon from 47.5% retention for MNS, to 11.6% for Mg to 2.6% for CF. S was removed to the smallest extent as retentions of 61, 72 and 91% were found for MNS, M50-C50 and CF respectively, which is attributed to the incorporation of S heteroatoms in the aromatic carbon structure, limiting its solubility in inorganic acids. However, the difference, the increase in mesoporosity for MNS and M50-

C50 and in microporosity for CF cannot be explained by the retention of certain inorganic species. Porosity during activation would be created by the inorganic compounds acting as hard templates on the carbon structures which would be removed after washing, leaving imprints (mesopores) behind [42]. One possibility would be that the chemical nature and crystallographic size of the present minerals would be different which would result in different behavior, however further research would be required to answer this question.

The demineralization of the activated carbons successfully removed large fractions of the ash. Moreover, increases in mesoporosity were observed for MNS and M50-C50. Ultimately this led to three activated carbons which had varying properties, the demineralized MNS and M50-C50 had well-developed micro-and meso-porous structure. Moreover, CF and M50-C50 contained substantial quantities of nitrogen after demineralization. This made the activated carbons interesting subjects for testing as an electrode material in a supercapacitor.

Cyclic voltammetry (CV) measurements were performed to assess the specific capacitance of the electrode materials against that of a reference commercial coconut shell based activated carbon (Comm). The specific capacitances of the washed and unwashed activated carbons were measured over a wide range of scan rates (1-100 mV/s), Figure 5.

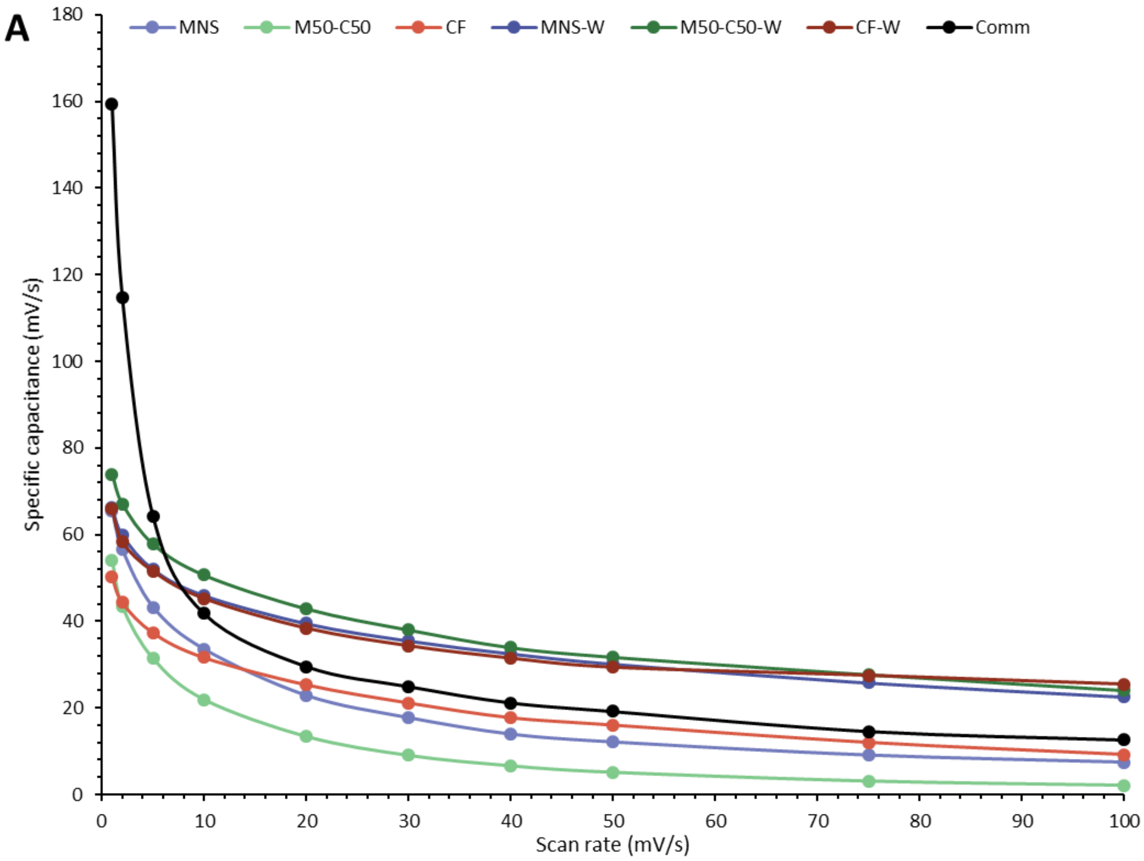

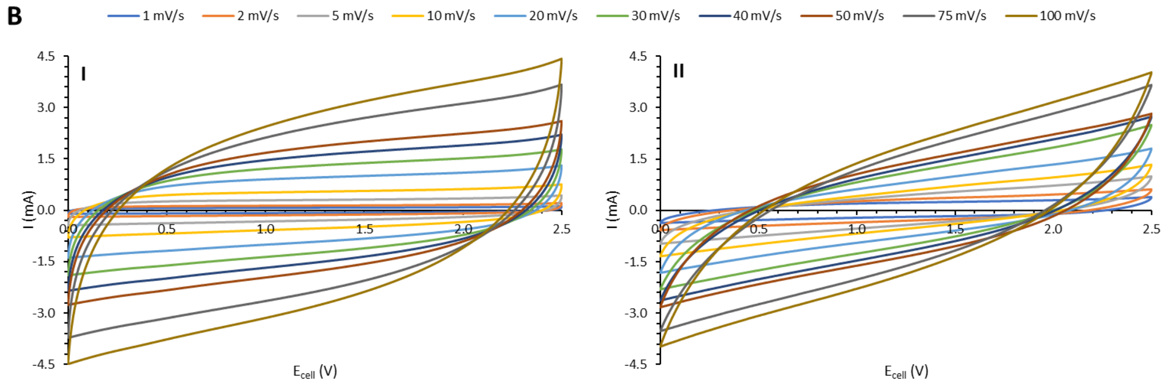

Figure 5: A) Specific capacitance versus scan rate for symmetric coin cells B) Cyclic voltammograms for (I) M50-C50-W and (II) Comm at different scan rates

At low scan rates the commercial activated carbon performed best, culminating in a specific capacitance of 159 F/g at a scan rate of 1 mV/s. At the same scan rate, the unwashed activated carbons were ranked from high to low as MNS 66 F/g, M50-C50 54 F/g and CF 50 F/g. Washing the activated carbons increased their specific capacitances, the greatest effects were observed for the nitrogen-containing activating carbons, for CF the specific capacitance increased up to 66 F/g, for M50-C50 the increase was up to 74 F/g. For MNS no increase in the specific capacitance was observed and the specific capacitance remained at 66 F/g at a scan rate of 1 mV/s, which indicated that the electrochemically active surface area for MNS did not change after washing. This contrasts with the behavior of nitrogen-containing carbons where an increase of micropore volume led to an increased specific capacitance at a scan rate of 1 mV/s (Figures 3 and 4). This result identifies the washed co-pyrolysis activated carbon as the best performing sample thanks to its well-developed porosity and favorable nitrogen-content increasing the electrochemically available active surface area.

Increasing the scan rates lowered the overall specific capacitance, this is due to the charge transport limitations which scales with the scan rate [43]. The activated carbons derived from CF and MNS showed both a meso- and microporous structure. This large meso-porosity would facilitate the flux of ions towards the mesopores at higher scan rates which results in the observed larger capacitance compared to other samples. Commercial devices are tested and utilized using higher currents or scan rates ~~[44]~~ (scan rates > 10 mV/s) at which all demineralized CF and MNS derived activated carbons demonstrate a better compared to the commercial activated carbon [44]. Specific capacitances of 43, 39 and 38 F/g were measured for M50-C50, MNS and CF after washing, respectively, compared to 30 F/g for the commercial activated carbon at 20 mV/s. Moreover, the shape of the CV-curve is less slanted for the meso-and microporous carbons compared to the microporous commercial benchmark, which indicates an increased contribution of capacitive charge storage (Figure 5B).

Lastly, the unwashed activated carbons all performed worse than the commercial reference, this would be due to the inorganic compounds blocking the pores and impeding an efficient charge transport [13].

Galvanostatic charge-discharge experiments were performed using different currents to further verify the finding that the washed activated carbons performed better than the commercial reference, (Figure 6).

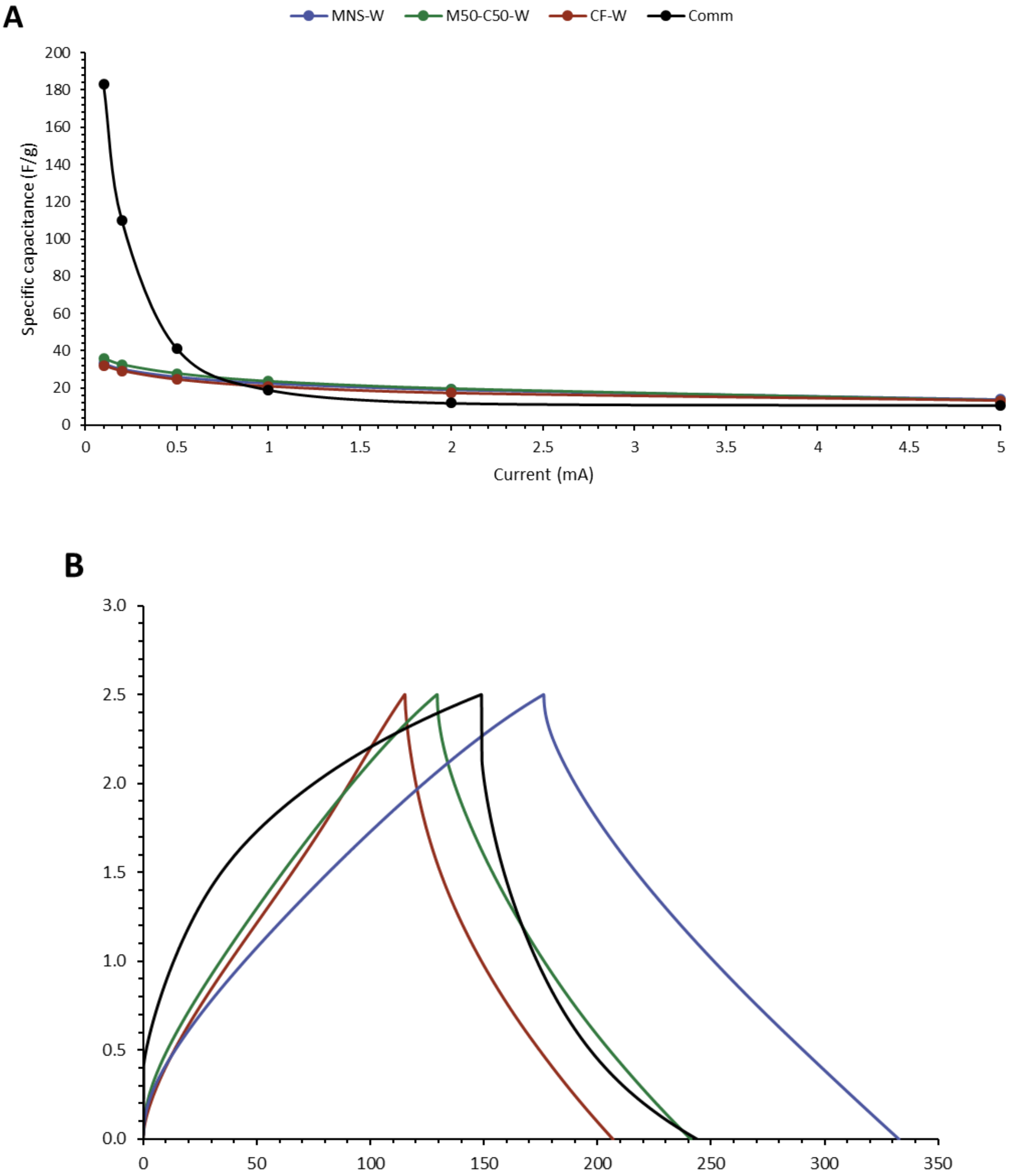

Figure 6: Specific capacitance versus current measured in the galavanostatic (GCD) tests for the samples X and Y …., A) over the current range of 0.1-5 mA B) used current 1mA

A similar trend regarding decreased specific capacitance with faster charge/discharge is observed for the charge-discharge curves, similarly as observed in cyclic voltammetry. When the current is increased above 1 mA (corresponding to around 0.1 A/g), the specific capacitance of the washed activated carbons exceeded those of the commercial activated carbon, measured capacitances were 16.2 F/g for Comm, 17.6 F/g for CF, 19.2 F/g for MNS and 20 F/g for M50-C50. In this case a small improvement in specific capacitance was observed for the co-pyrolysis activated carbons, owing to its well-developed porosity and adequately large nitrogen content. In future practical applications, a higher charge-rate is required, as typically supercapacitors are charged and discharged in a matter of seconds to at most several minutes, therefore the very low scan rates and current densities are appropriate to uncover maximal specific capacitances of a certain material but they do not reflect practical device behavior [45]. From the ratio of voltage drop (ΔV) over current change upon discharge ($2I$) the Internal resistance of the coin cells could be calculated. These were 40.8, 34.7 and 31.5 Ω for CF, M50-C50 and MNS, respectively, after demineralization, being significantly lower than the internal resistance of the commercial activated carbon (185 Ω at 1 mA). To obtain more in-depth information on the impedance characteristics of the supercapacitor coin cells, electrochemical impedance spectroscopy was carried out (Figure 7).

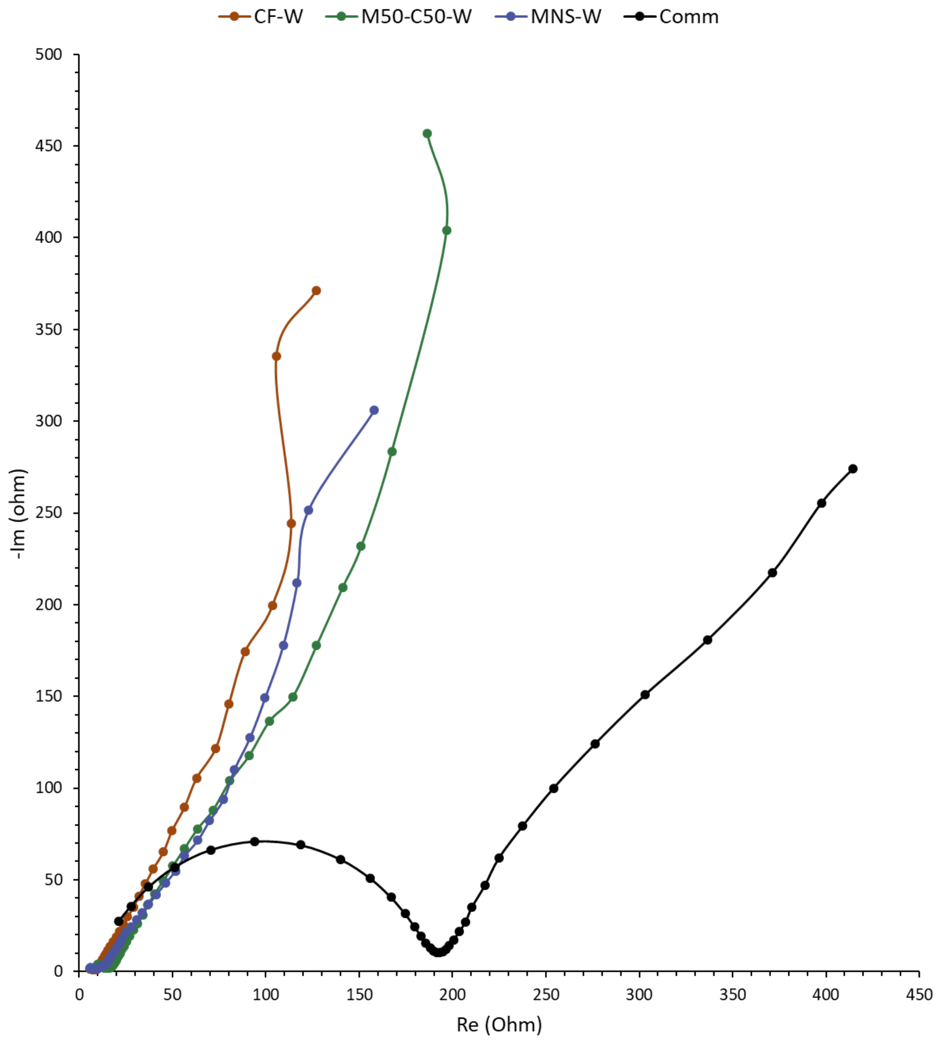

Figure 7: Potentiostatic electrochemical impedance spectroscopy (amplitude 5 mV)

Three types of resistance limitations could be observed from the impedance spectra. Firstly, the equivalent series resistance at high frequency (the ohmic resistance of the complete cell with all its parts) was found to be similar for the three carbons (5.8, 9.9 and 5.7 Ω for CF, M50-C50 and MNS respectively) and smaller compared to the commercial activated carbon 21 Ω. Moreover, all three demineralized activated carbons showed good compatibility with the EC/DEC electrolyte surface as the interfacial impedance is low, evidenced by the absence of the characteristic semi-circle [46], which is clearly pronounced for the commercial activated carbon (Figure 7). The interfacial impedance of activated carbon is determined by the diffusion rate of the ions inside electrolyte towards the micropores, hence this could be improved by the presence of mesopore channels in the activated carbons or by the presence of heteroatoms on the activated carbon surface which increases the wettability of the electrodes [22]. At low frequencies the impedance is dominated by the more sluggish phenomena such as diffusion within the micropores reflected in the steady rise of imaginary part of the impedance [46]. This is similar for all four tested activated carbons as all samples contain a certain quantity of accessible micropores. One of the most important supercapacitor properties is their cycling stability, which was tested for 10 000 cycles (Figure 8).

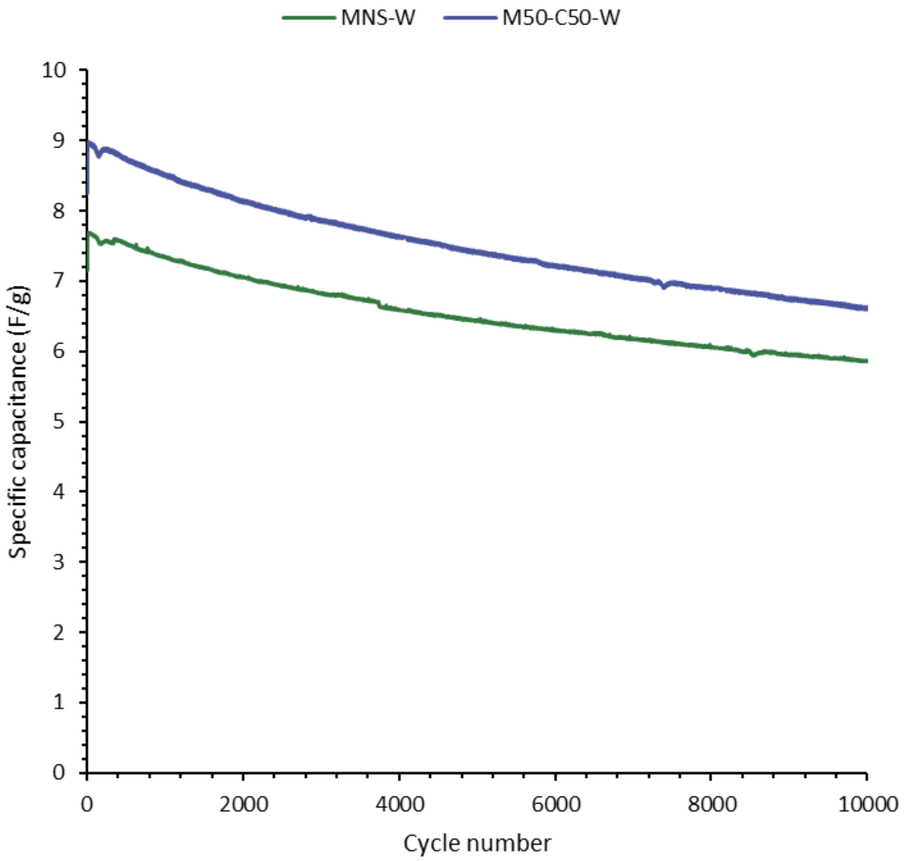

Figure 8: Cycling stability of MNS-W and M50-C50-W using a current density of 1 A/g and a voltage window 0-2.5 V

The cycling stability of the washed activated carbons was assessed over 10 000 cycles at 1 A/g. The washed CF activated carbon malfunctioned after 120 cycles, therefore this sample is not displayed in Figure 8 but added in supplementary material (Figure S3). One of the possible reasons for its malfunctioning is its high oxygen content (18 wt%) which could have caused the formation of irreversible redox reactions with the organic electrolyte, resulting in electrolyte degradation and formation of gaseous products, ultimately leading to device failure [47]. M50-C50 and MNS-based supercapacitors could be effectively cycled for the desired testing period. Both showed moderate capacitance retentions of 73.5% and 76.2% for M50-C50 and MNS, respectively, after 10 000 cycles. In terms of specific capacitance this corresponds to 5.9 F/g and 6.6 F/g for MNS and M50-C50, respectively. The decrease in the specific capacitance over the cycling period might be associated with the irreversible charge transfer reactions happening, also due to the presence of oxygen on the carbon surface. Previous research has shown that cycling oxygen-rich activated carbons in organic electrolytes leads to the electrolyte degradation. The resulting degradation products would accumulate in the activated carbon’s pores which would lower the electrochemically available surface area and subsequently the specific capacitance of the material [48]. One of the proposed strategies which could have improved the functionality of the activated carbon’s in organic electrolytes would have been a high-temperature annealing step to remove surface oxygen groups. Ultimately, CF-MNS based activated carbons have shown promising initial potential to be used as electrode materials in activated carbons, due to a good combination of meso- and micro-porosity.

4 Conclusions

Co-pyrolyzing and physically activating CF and MNS yields promising nitrogen-rich activated carbon which can be applied in supercapacitor devices. The co-pyrolysis increased the nitrogen retention during the pyrolysis from 9% to 18% compared to CF pyrolysis. Moreover, the porous characteristics of the blended activated carbons were comparable to those of MNS, yielding a good mix of micro- and mesopores. Moreover, demineralization increased both meso-and microporosity of this activated carbon, which resulted in a specific capacitance of 66 F/g at 1 mV/s, which was lower than a commercial activated carbon 159 mV/s. Nevertheless, at higher scan rates (20 mV/s) the co-pyrolysis activated carbon outperformed the commercial, 43 versus 30 F/g, thanks to its abundance of mesopores which enabled fast charge delivery. Lastly, cycling stability tests showed a moderate stability of 73% of capacitance retention over 10000 cycles at 1 A/g for ? sample. The addition of an annealing step to remove oxygen functionalities was proposed as a strategy to improve the cycling stability.

References

[1] B. Grizzetti, U. Pretato, L. Lassaletta, G. Billen, J. Garnier, The contribution of food waste to global and European nitrogen pollution, Environ. Sci. Policy. 33 (2013) 186–195. https://doi.org/10.1016/J.ENVSCI.2013.05.013.

[2] B. Ramakrishnan, N.R. Maddela, K. Venkateswarlu, M. Megharaj, Potential of microalgae and cyanobacteria to improve soil health and agricultural productivity: a critical view, Environ. Sci. Adv. (2023) 586–611. https://doi.org/10.1039/d2va00158f.

[3] G. Su, H.C. Ong, I.M.R. Fattah, Y.S. Ok, J.-H. Jang, C.-T. Wang, State-of-the-art of the pyrolysis and co-pyrolysis of food waste: Progress and challenges, Sci. Total Environ. 809 (2022) 151170. https://doi.org/10.1016/j.scitotenv.2021.151170.

[4] F. and A.O. of the U. Nations, World Food and Agriculture – Statistical Yearbook 2022, FAO, 2022. https://doi.org/10.4060/cc2211en.

[5] K.N. Wood, R. O'Hayre, S. Pylypenko, Recent progress on nitrogen/carbon structures designed for use in energy and sustainability applications, in: Energy Environ. Sci., Royal Society of Chemistry, 2014: pp. 1212–1249. https://doi.org/10.1039/c3ee44078h.

[6] Z. Zhao, Y. Wang, M. Li, R. Yang, High performance N-doped porous activated carbon based on chicken feather for supercapacitors and CO 2 capture, RSC Adv. 5 (2015) 34803–34811. https://doi.org/10.1039/C5RA01569C.

[7] E. Hastuti, A. Subhan, D. Puspitasari, Synthesis of activated carbon derived from chicken feather for Li-ion batteries through chemical and physical activation process, Mater. Renew. Sustain. Energy. 10 (2021) 13. https://doi.org/10.1007/s40243-021-00198-6.

[8] H. Chen, R. Shan, F. Zhao, J. Gu, Y. Zhang, H. Yuan, Y. Chen, A review on the NOx precursors release during biomass pyrolysis, Chem. Eng. J. 451 (2023) 138979. https://doi.org/10.1016/j.cej.2022.138979.

[9] X. Wang, D. Ma, Q. Jin, S. Deng, H. Stančin, H. Tan, H. Mikulčić, Synergistic effects of biomass and polyurethane co-pyrolysis on the yield, reactivity, and heating value of biochar at high temperatures, Fuel Process. Technol. 194 (2019). https://doi.org/10.1016/j.fuproc.2019.106127.

[10] D. Xu, L. Yang, M. Zhao, Y. Song, Karnowo, H. Zhang, X. Hu, H. Sun, S. Zhang, N Evolution and Physiochemical Structure Changes in Chars during Co-Pyrolysis: Effects of Abundance of Glucose in Fiberboard, Energies. 13 (2020) 5105. https://doi.org/10.3390/en13195105.

[11] W. Chen, Y. Chen, H. Yang, M. Xia, K. Li, X. Chen, H. Chen, Co-pyrolysis of lignocellulosic biomass and microalgae: Products characteristics and interaction effect, Bioresour. Technol. 245 (2017) 860–868. https://doi.org/10.1016/j.biortech.2017.09.022.

[12] P. Monkhouse, On-line diagnostic methods for metal species in industrial process gas, 2002. https://doi.org/10.1016/S0360-1285(02)00006-0.

[13] R. Mehdi, A.H. Khoja, S.R. Naqvi, N. Gao, N.A.S. Amin, A Review on Production and Surface Modifications of Biochar Materials via Biomass Pyrolysis Process for Supercapacitor Applications, Catalysts. 12 (2022) 798. https://doi.org/10.3390/catal12070798.

[14] K. Kierzek, G. Gryglewicz, Activated Carbons and Their Evaluation in Electric Double Layer Capacitors, Molecules. 25 (2020) 4255. https://doi.org/10.3390/molecules25184255.

[15] X. Lu, K. Xiang, W. Zhou, Y. Zhu, Y. He, H. Chen, Graphene-Like Carbon Derived from Macadamia Nut Shells for High-Performance Supercapacitor, Russ. J. Electrochem. 55 (2019) 242–246. https://doi.org/10.1134/S1023193519020034.

[16] Z. Li, Q. Liang, C. Yang, L. Zhang, B. Li, D. Li, Convenient preparation of nitrogen-doped activated carbon from Macadamia nutshell and its application in supercapacitor, J. Mater. Sci. Mater. Electron. 28 (2017) 13880–13887. https://doi.org/10.1007/s10854-017-7236-4.

[17] X. Yan, Y. Jia, L. Zhuang, L. Zhang, K. Wang, X. Yao, Defective Carbons Derived from Macadamia Nut Shell Biomass for Efficient Oxygen Reduction and Supercapacitors, ChemElectroChem. 5 (2018) 1874–1879. https://doi.org/10.1002/celc.201800068.

[18] P.A. Shinde, Q. Abbas, N.R. Chodankar, K. Ariga, M.A. Abdelkareem, A.G. Olabi, Strengths, weaknesses, opportunities, and threats (SWOT) analysis of supercapacitors: A review, J. Energy Chem. 79 (2023) 611–638. https://doi.org/10.1016/j.jechem.2022.12.030.

[19] K. Tian, J. Wang, L. Cao, W. Yang, W. Guo, S. Liu, W. Li, F. Wang, X. Li, Z. Xu, Z. Wang, H. Wang, Y. Hou, Single-site pyrrolic-nitrogen-doped sp2-hybridized carbon materials and their pseudocapacitance, Nat. Commun. 11 (2020) 3884. https://doi.org/10.1038/s41467-020-17727-y.

[20] A. Barroso Bogeat, Understanding and Tuning the Electrical Conductivity of Activated Carbon: A State-of-the-Art Review, Crit. Rev. Solid State Mater. Sci. 46 (2021) 1–37. https://doi.org/10.1080/10408436.2019.1671800.

[21] W. Dong, M. Xie, S. Zhao, Q. Qin, F. Huang, Materials design and preparation for high energy density and high power density electrochemical supercapacitors, Mater. Sci. Eng. R Reports. 152 (2023) 100713. https://doi.org/10.1016/j.mser.2022.100713.

[22] A. Gopalakrishnan, S. Badhulika, Effect of self-doped heteroatoms on the performance of biomass-derived carbon for supercapacitor applications, J. Power Sources. 480 (2020) 228830. https://doi.org/10.1016/j.jpowsour.2020.228830.

[23] M. Cossutta, V. Vretenar, T.A. Centeno, P. Kotrusz, J. McKechnie, S.J. Pickering, A comparative life cycle assessment of graphene and activated carbon in a supercapacitor application, J. Clean. Prod. 242 (2020) 118468. https://doi.org/10.1016/j.jclepro.2019.118468.

[24] K. Vanreppelen, S. Vanderheyden, T. Kuppens, S. Schreurs, J. Yperman, R. Carleer, Activated carbon from pyrolysis of brewer’s spent grain: Production and adsorption properties, Waste Manag. Res. 32 (2014) 634–645. https://doi.org/10.1177/0734242X14538306.

[25] W. Vercruysse, J. Smeets, T. Haeldermans, B. Joos, A. Hardy, P. Samyn, J. Yperman, K. Vanreppelen, R. Carleer, P. Adriaensens, W. Marchal, D. Vandamme, Biochar from raw and spent common ivy: Impact of preprocessing and pyrolysis temperature on biochar properties, J. Anal. Appl. Pyrolysis. 159 (2021) 105294. https://doi.org/10.1016/j.jaap.2021.105294.

[26] W. Vercruysse, C. Laurino Gomes, D. Bleus, M. Pappa, B. Joos, A. Hardy, W. Marchal, D. Vandamme, Demineralization of common ivy-derived biomass and biochar and its effect on the resulting activated carbon properties, Sep. Purif. Technol. 319 (2023) 124023. https://doi.org/10.1016/j.seppur.2023.124023.

[27] ASTM International, Standard Test Method for Total Ash Content of Activated Carbon, ASTM Stand. 15 (2004) 1–2. https://doi.org/10.1520/D2866-11.2.

[28] G.K. Wertheim, S.B. Dicenzo, Least-squares analysis of photoemission data, J. Electron Spectros. Relat. Phenomena. 37 (1985) 57–67. https://doi.org/10.1016/0368-2048(85)80082-7.

[29] M. Ayiania, M. Smith, A.J.R. Hensley, L. Scudiero, J.S. McEwen, M. Garcia-Perez, Deconvoluting the XPS spectra for nitrogen-doped chars: An analysis from first principles, Carbon N. Y. 162 (2020) 528–544. https://doi.org/10.1016/j.carbon.2020.02.065.

[30] K. Mainali, M. Garcia-Perez, Understanding organic N interactions with cellulose during pyrolysis to produce N-doped carbonaceous materials, J. Anal. Appl. Pyrolysis. 169 (2023) 105791. https://doi.org/10.1016/j.jaap.2022.105791.

[31] L.D. Mafu, H.W.J.P. Neomagus, R.C. Everson, C.A. Strydom, M. Carrier, G.N. Okolo, J.R. Bunt, Chemical and structural characterization of char development during lignocellulosic biomass pyrolysis, Bioresour. Technol. 243 (2017) 941–948. https://doi.org/10.1016/j.biortech.2017.07.017.

[32] W.-J. Liu, W.-W. Li, H. Jiang, H.-Q. Yu, Fates of Chemical Elements in Biomass during Its Pyrolysis, Chem. Rev. 117 (2017) 6367–6398. https://doi.org/10.1021/acs.chemrev.6b00647.

[33] J.R. Pels, F. Kapteijn, J.A. Moulijn, Q. Zhu, K.M. Thomas, Evolution of nitrogen functionalities in carbonaceous materials during pyrolysis, Carbon N. Y. 33 (1995) 1641–1653.

[34] X. Liu, S. Zuo, N. Cui, S. Wang, Investigation of ammonia/steam activation for the scalable production of high-surface area nitrogen-containing activated carbons, Carbon N. Y. 191 (2022) 581–592. https://doi.org/10.1016/J.CARBON.2022.02.014.

[35] M. Molina-Sabio, M.T. González, F. Rodriguez-Reinoso, A. Sepúlveda-Escribano, Effect of steam and carbon dioxide activation in the micropore size distribution of activated carbon, Carbon N. Y. 34 (1996) 505–509. https://doi.org/10.1016/0008-6223(96)00006-1.

[36] Y. He, Y. Zhang, X. Li, Z. Lv, X. Wang, Z. Liu, X. Huang, Capacitive mechanism of oxygen functional groups on carbon surface in supercapacitors, Electrochim. Acta. 282 (2018) 618–625. https://doi.org/10.1016/j.electacta.2018.06.103.

[37] C. Qiu, L. Jiang, Y. Gao, L. Sheng, Effects of oxygen-containing functional groups on carbon materials in supercapacitors: A review, Mater. Des. 230 (2023) 111952. https://doi.org/10.1016/j.matdes.2023.111952.

[38] A. Bazan-Wozniak, P. Nowicki, R. Pietrzak, The effect of demineralization on the physicochemical and sorption properties of activated bio-carbons, Adsorption. 25 (2019) 337–343. https://doi.org/10.1007/S10450-019-00009-5/FIGURES/5.

[39] W. Vercruysse, L.C. Gomes, D. Bleus, M. Pappa, B. Joos, A. Hardy, W. Marchal, D. Vandamme, Demineralization of common ivy-derived biomass and biochar and its effect on the resulting activated carbon properties, Sep. Purif. Technol. (2023).

[40] S.G. Krishnan, A. Arulraj, P. Jagadish, M. Khalid, M. Nasrollahzadeh, R. Fen, C.-C. Yang, G. Hegde, Pore size matters!—a critical review on the supercapacitive charge storage enhancement of biocarbonaceous materials, Crit. Rev. Solid State Mater. Sci. 48 (2023) 1–56. https://doi.org/10.1080/10408436.2022.2027225.

[41] J. Donald, Y. Ohtsuka, C. (Charles) Xu, Effects of activation agents and intrinsic minerals on pore development in activated carbons derived from a Canadian peat, Mater. Lett. 65 (2011) 744–747. https://doi.org/10.1016/j.matlet.2010.11.049.

[42] F. Ran, X. Yang, X. Xu, S. Li, Y. Liu, L. Shao, Green activation of sustainable resources to synthesize nitrogen-doped oxygen-riched porous carbon nanosheets towards high-performance supercapacitor, Chem. Eng. J. 412 (2021) 128673. https://doi.org/10.1016/J.CEJ.2021.128673.

[43] W. Qian, F. Sun, Y. Xu, L. Qiu, C. Liu, S. Wang, F. Yan, Human hair-derived carbon flakes for electrochemical supercapacitors, Energy Environ. Sci. 7 (2014) 379–386. https://doi.org/10.1039/C3EE43111H.

[44] J. Zhao, A.F. Burke, Review on supercapacitors: Technologies and performance evaluation, J. Energy Chem. 59 (2021) 276–291. https://doi.org/10.1016/j.jechem.2020.11.013.

[45] J. Huang, Y. Xie, Y. You, J. Yuan, Q. Xu, H. Xie, Y. Chen, Rational Design of Electrode Materials for Advanced Supercapacitors: From Lab Research to Commercialization, Adv. Funct. Mater. 2213095 (2023) 2213095. https://doi.org/10.1002/adfm.202213095.

[46] H.D. Yoo, J.H. Jang, J.H. Ryu, Y. Park, S.M. Oh, Impedance analysis of porous carbon electrodes to predict rate capability of electric double-layer capacitors, J. Power Sources. 267 (2014) 411–420. https://doi.org/10.1016/j.jpowsour.2014.05.058.

[47] R. Kötz, M. Hahn, P. Ruch, R. Gallay, Comparison of pressure evolution in supercapacitor devices using different aprotic solvents, Electrochem. Commun. 10 (2008) 359–362. https://doi.org/10.1016/j.elecom.2007.12.016.

[48] P. Azaïs, L. Duclaux, P. Florian, D. Massiot, M.-A. Lillo-Rodenas, A. Linares-Solano, J.-P. Peres, C. Jehoulet, F. Béguin, Causes of supercapacitors ageing in organic electrolyte, J. Power Sources. 171 (2007) 1046–1053. https://doi.org/10.1016/j.jpowsour.2007.07.001.

Supplementary information

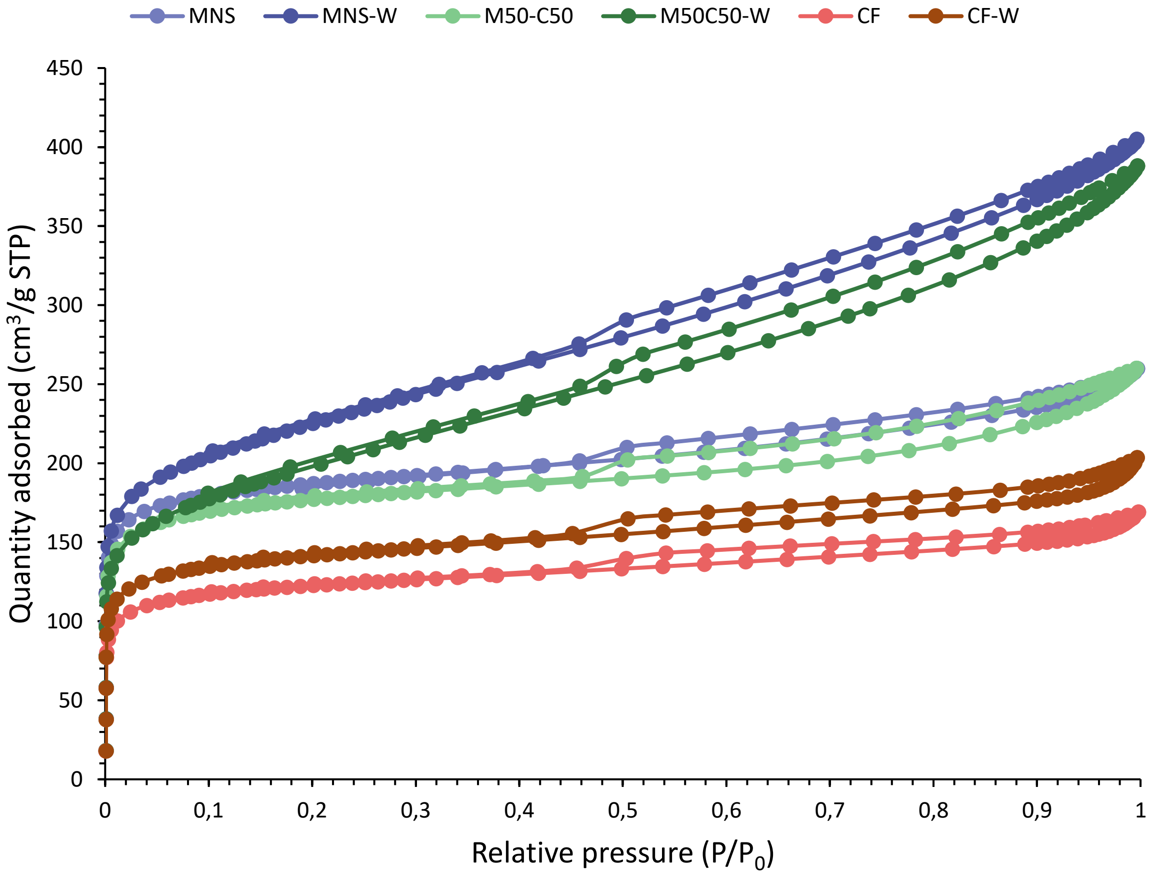

Figure S1: Nitrogen physisorption isotherms of demineralized and pristine activated carbons

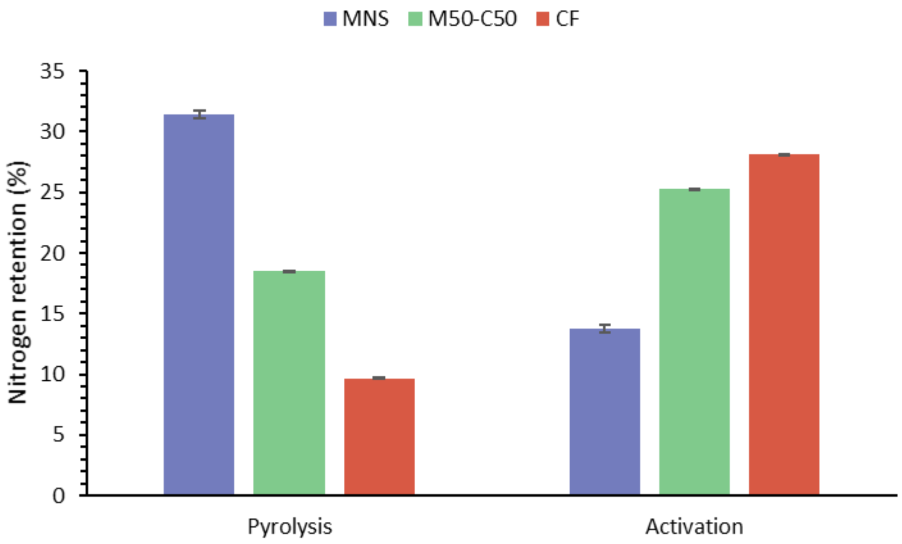

Figure S2: Nitrogen retentions during thermochemical conversion

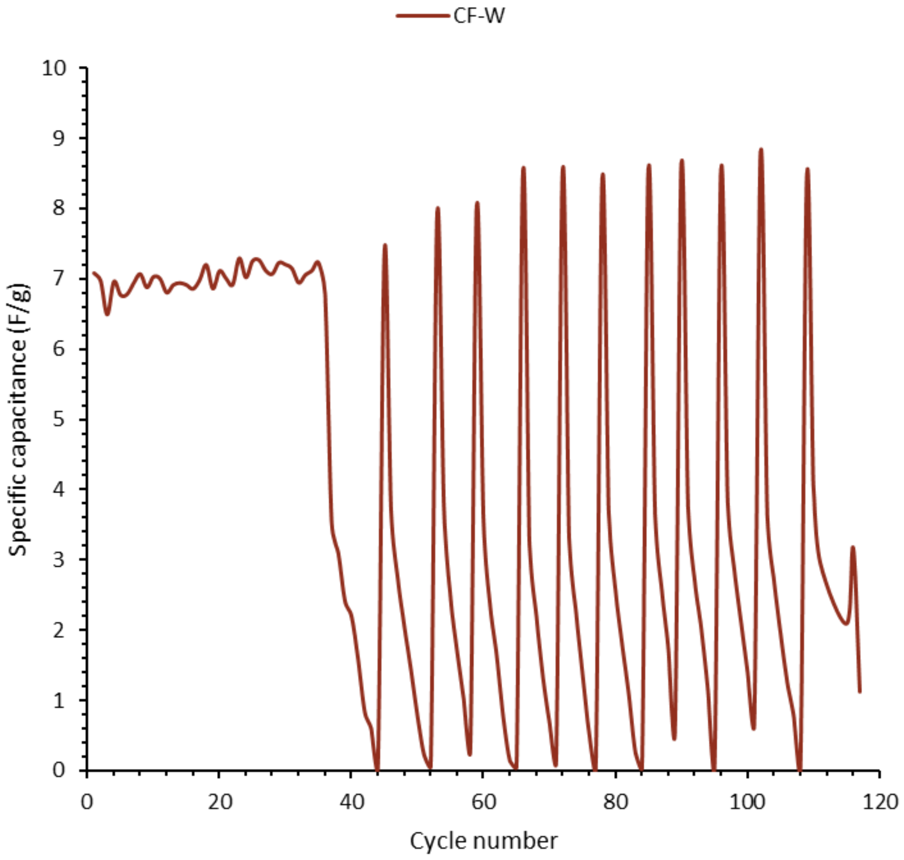

Figure S3: Cycling stability of CF-W (1 A/g, voltage window 0-2.5 V)